Earth Planet. Sci. Lett. 660 (2025) 119346

Contents lists available at ScienceDirect

Earth and Planetary Science Letters

journal homepage: www.elsevier.com/locate/epsl

Stable tungsten (W) isotope systematics in marine sediments: a potential paleo-proxy for deep ocean oxygenation

Ruiyu Yang [a,b,*], Marcus Gutjahr [b], Florian Scholz [c], Florian Kurzweil [a], Sümeyya Eroglu [d], Carsten Münker [a]

[a] Institute of Geology and Mineralogy, University of Cologne, Cologne 50674, Germany
[b] GEOMAR Helmholtz Centre for Ocean Research Kiel, Kiel 24148, Germany
[c] Institute for Geology, Center for Earth System Research and Sustainability, University of Hamburg, Hamburg 20146, Germany
[d] Institute of Geology and Paleontology, University of Münster, Münster 48149, Germany

ARTICLE INFO

Editor: Dr H Bao

Key words:
Stable tungsten isotopes
Early diagenesis
Manganese oxides
Continental margin settings
Manganese cycling
Molybdenum

ABSTRACT

The stable tungsten (W) isotope system has emerged as a promising paleoenvironmental indicator. However, the modern oceanic budget of W and its behavior during sedimentary burial are to date not well understood. Specifically, the mechanisms governing W delivery to marine sediments and its behavior during early diagenesis remain unknown. In this study, we analyzed stable W isotopic compositions ($\delta^{186/184}$W) in three sediment cores from various redox environments in the Gulf of California. Additionally, we investigated $\delta^{186/184}$W compositions and major and trace elemental compositions in surface sediments from global ocean basins. Our findings indicate that continental margin sediments and hydrothermal precipitates lack significant authigenic W enrichment, whereas deep-ocean surface sediments exhibit notable W enrichment, primarily associated with Mn-oxides. Tungsten appears to be delivered alongside Mn but does not undergo burial under anoxic or euxinic conditions, unlike its geochemical counterpart, Mo. The tungsten output flux into total Mn oxides is estimated at 22.2 $\times$ 10^6 mol/yr. Authigenic W (excess W relative to the detrital input) exhibits heavier W isotope compositions compared to equilibrium adsorption on Mn oxides from modern seawater, averaging a $\delta^{186/184}$W of 0.255 $\pm$ 0.025 ‰. This is likely due to fractionation processes during continuous exchange between pore-water and the solid phase, or the recrystallization of Mn oxides during diagenesis. Finally, we propose an updated mass budget of W and its isotopes in the modern ocean suggesting that the benthic W recycling could be an important, so far underestimated source of W to the ocean. The exclusive association between W and Mn suggests that W isotopes could serve as a valuable indicator for identifying deep-ocean oxygenation in Earth's history. To advance this idea, further comprehensive investigations into W isotopic fractionation across various Fe and Mn oxide minerals, as well as additional downcore studies in authigenic W enriched pelagic core sites, would be essential.

1. Introduction

The abundance of oxygen in the atmosphere and oceans is essential for the development of complex life forms, making the evolution of oxygenation a critical area of research in Earth's evolution. Redox-sensitive elements offer valuable insights in addressing this research field (Bennett and Canfield, 2020; Brumsack, 2006; Scholz, 2018; Tribovillard et al., 2006). Tungsten (W) and its isotopes, to date still representing under-utilized redox proxies, have the potential to further our understanding of Earth's oxygenation history (e.g., Dellwig et al., 2019; Kurzweil et al., 2021; Roué et al., 2021; Yang et al., 2023). Tungsten and its geochemical twin, molybdenum (Mo), are both redox sensitive and are part of the chromium group in the periodic table. Under oxic conditions, both elements form oxyanions and are readily adsorbed onto Fe-Mn oxyhydroxides (Kashiwabara et al., 2013). In sulfidic environments, both W and Mo undergo thiolation, although thiolation of W requires higher sulfide concentrations (Cui et al., 2021). Both experimental and field observations have indicated that stable W isotope compositions undergo fractionation during transport and sedimentation through interactions involving adsorption to and release from Fe-Mn oxyhydroxides (Kashiwabara et al., 2017; Kurzweil et al., 2021; Yang et al., 2023). This isotopic fractionation is ascribed to changes in bond

* Corresponding author.
E-mail address: ryang2@uni-koeln.de (R. Yang).

https://doi.org/10.1016/j.epsl.2025.119346
Received 13 January 2025; Received in revised form 28 March 2025; Accepted 31 March 2025
Available online 7 April 2025

strength resulting from coordination changes (Kashiwabara et al., 2017). Such fractionation, reflective of redox variations, also influences the isotope signature of seawater W, which may be preserved in sediments.

Tungsten in seawater primarily originates from continental weathering and is transported to the ocean by riverine inputs, with an average riverine W isotope composition ($\delta^{186/184}W$) of 0.37 ± 0.04 ‰ (Yang et al., 2022). The main sink for W in the ocean are oxic sediments, whereas anoxic sediments in euxinic basins do not make a significant contribution to W burial (Yang et al., 2022). The dissolved concentration of W in the ocean is quite low, typically in the picomolar range at around 41–67 pM (Firdaus et al., 2008; Sohrin et al., 1987). The isotopic composition of W in oxic seawater is widely considered to be uniform globally, generally averaging 0.543 ± 0.046 ‰ (Fujiwara et al., 2020; Kurzweil et al., 2021). The residence time for W in the modern ocean has been estimated at ~4000 years (Yang et al., 2022), which is longer than the global ocean mixing time of ~1000 years, suggesting a tendency toward relative global homogeneity of both W isotope compositions and salinity-normalized W concentrations in open ocean seawater. Relatively recent pioneering studies have employed stable W isotopes as an indicator of paleo-environmental conditions, spanning the geological timescales from the Archean to the late Miocene (Alam et al., 2022; Roué et al., 2021; Yang et al., 2023). Nevertheless, the utility of stable W isotopes as a proxy for paleo-environmental reconstruction ultimately depends on a comprehensive understanding of the mechanisms governing W transfer from seawater to sediments and the influence of post-depositional diagenetic processes within the present-day ocean system. Only a few studies on stable W isotopes have focused on localized marine environments, such as sediment cores from the Arabian Sea (Alam et al., 2022), the Baltic Sea (Kurzweil et al., 2022), the Japan Sea (Tsujisaka et al., 2020), and deep-sea ferromanganese crusts from the Pacific Ocean (Yang et al., 2023). However, sediments from continental margins and global ocean basins have not been extensively explored for the W isotope system. Studies integrating multiple isotope systems allow refining our understanding of past environmental conditions and enhance the reliability of their reconstructions. Linking the Mo and W isotope systems hence emerges as a promising path. Nevertheless, the connections between $\delta^{186/184}W$ and $\delta^{98/95}Mo$ compositions, as well as the concurrent fractionation variations during sedimentary burial for these two isotope systems, are yet to be fully understood.

Additionally, the behavior of W within hydrothermal systems has not been extensively characterized to date. Kishida et al. (2004) provided the only direct measurements of W concentrations in hydrothermal vent fluids, revealing variably higher levels than those in ambient seawater. The disparities in W concentrations are primarily due to the types of rocks involved in fluid-rock interactions. Specifically, calc-alkaline dacite and terrigenous sediments are the primary W contributors in the studied area. Yang et al. (2022) estimated the maximum global hydrothermal inputs, utilizing ratios of W/Sr in mid-ocean ridge basalt (MORB) and the Sr flux. For the maximum estimation of hydrothermal outputs, the authors used W contents in average seawater and the water flux through hydrothermal systems, assuming extreme cases that all W is removed by hydrothermal activity, such as hydrothermal vent precipitation, oceanic alteration, secondary mineral formation, and scavenging by hydrothermal plumes. They concluded that hydrothermal contributions are negligible compared to riverine inputs. However, the sediments deposited near hydrothermal vents, which could provide direct evidence of hydrothermal processes, have not been investigated for their W concentration and isotope compositions.

The overall objective of this study is to investigate and compare the behavior of W and its isotopes in sediment cores extending from continental margins to global ocean basins. Specifically, we aim to provide new constraints for the W budget in the modern ocean and to seek possibilities for the application of W isotopes as a paleo-environmental proxy. Three sediment cores from the Gulf of California were examined: one from the oxygenated deep Guaymas Basin with significant Mn enrichment, one from the oxygen minimum zone (OMZ), and one from a hydrothermal vent field. Additionally, 47 surface sediments from globally distributed sites in all major ocean basins were analyzed to understand the behavior of W during early diagenesis and the impact of post-depositional processes on the W isotope composition that becomes part of the paleo-record. Finally, we revisit the global W budget and explore the potential of W isotopes as a tool for deciphering redox conditions and Mn cycling in Earth's history.

2. Samples and methods

2.1. Sample materials

Continental margin sediments were collected from the Guaymas Basin in the Gulf of California using a multi corer (MUC) during the *R.V. Sonne* SO241 scientific cruise (Fig. 1). The Guaymas Basin, an expansive rift basin approximately 100 km wide and 2200 m deep, is situated within the Gulf of California, between mainland Mexico and the Baja California peninsula. This region experiences climatic seasonality: predominant northwesterly winds induce overturning of the water column from late autumn to early spring, resulting in nutrient upwelling and elevated phytoplankton production. Conversely, steady southward winds during summer and early autumn create a monsoonal climate characterized by increased rainfall and decreased primary productivity (Barron et al., 2004; Marinone, 2003). Due to the decomposition of sinking organic matter at intermediate depth and the influx of oxygen-depleted Pacific Intermediate Water (PIW) into the Gulf, a pronounced OMZ is present at depths between 500 and 1000 m (Bray, 1988; Thunell, 1998).

The Guaymas Basin's geology is characterized by active spreading along the ocean floor, interconnected with spreading centers and transform faults that originate from the East Pacific Rise (EPR). This tectonic activity has led to distinctive graben structures and the emergence of hydrothermal vent fields (Berndt et al., 2016; Simoneit et al., 1988). In this study, three distinct sediment cores representing variable redox states and depositional environments were investigated (Fig. 1b). Core MUC3 (27°23.827′ N, 111°25.923′ W, 2043 m), referred to as the graben core, was deposited in a graben-shaped seafloor environment with weakly oxygenated bottom water (~37 μM O_2) and abundant Mn supply from ambient hydrothermal vents and surrounding slopes. Sediments in core MUC9 (27°42.410′ N, 111°13.656′ W, 667 m), situated within the OMZ, settled under anoxic bottom water conditions (< 2 μM O_2). Core MUC16 (27°24.577′ N, 111°23.265′ W, 1853 m), referred to as the vent-related core, with ~25 μM O_2 in bottom water, was retrieved near hydrothermal vents and specifically adjacent to active black smokers. It consists of black smoker debris characterized by high Fe concentrations.

Additionally, surface sediments from global ocean basins were investigated. In total, 47 sediment samples were obtained from the GEOMAR Core & Rock Repository (Fig. 1), collected during multiple cruises to the Pacific, Atlantic, Indian, Southern Oceans, as well as Black Sea, encompassing diverse sedimentary settings such as mid-oceanic ridges, hydrothermal vents, continental margins, abyssal plains, and marginal seas. All these samples represent core-top sediments (<1 cm depth). Coring details and concise sample descriptions are provided in Table S1. By following these selection criteria, we ensured that these sediments were deposited from modern or recent seawater and avoid potential temporal variations in seawater compositions that may be recorded in older sediments at greater depth. Considering the residence time of W in modern seawater, which exceeds the ocean mixing time, and the consistency of $\delta^{186/184}W$ observed in seawater samples measured at different locations, the global seawater $\delta^{186/184}W$ composition is considered homogeneous (Fujiwara et al., 2020; Kurzweil et al., 2021). Where possible, multiple sampling sites were selected for most basins to capture variations and enable comparison within the same depositional environment.

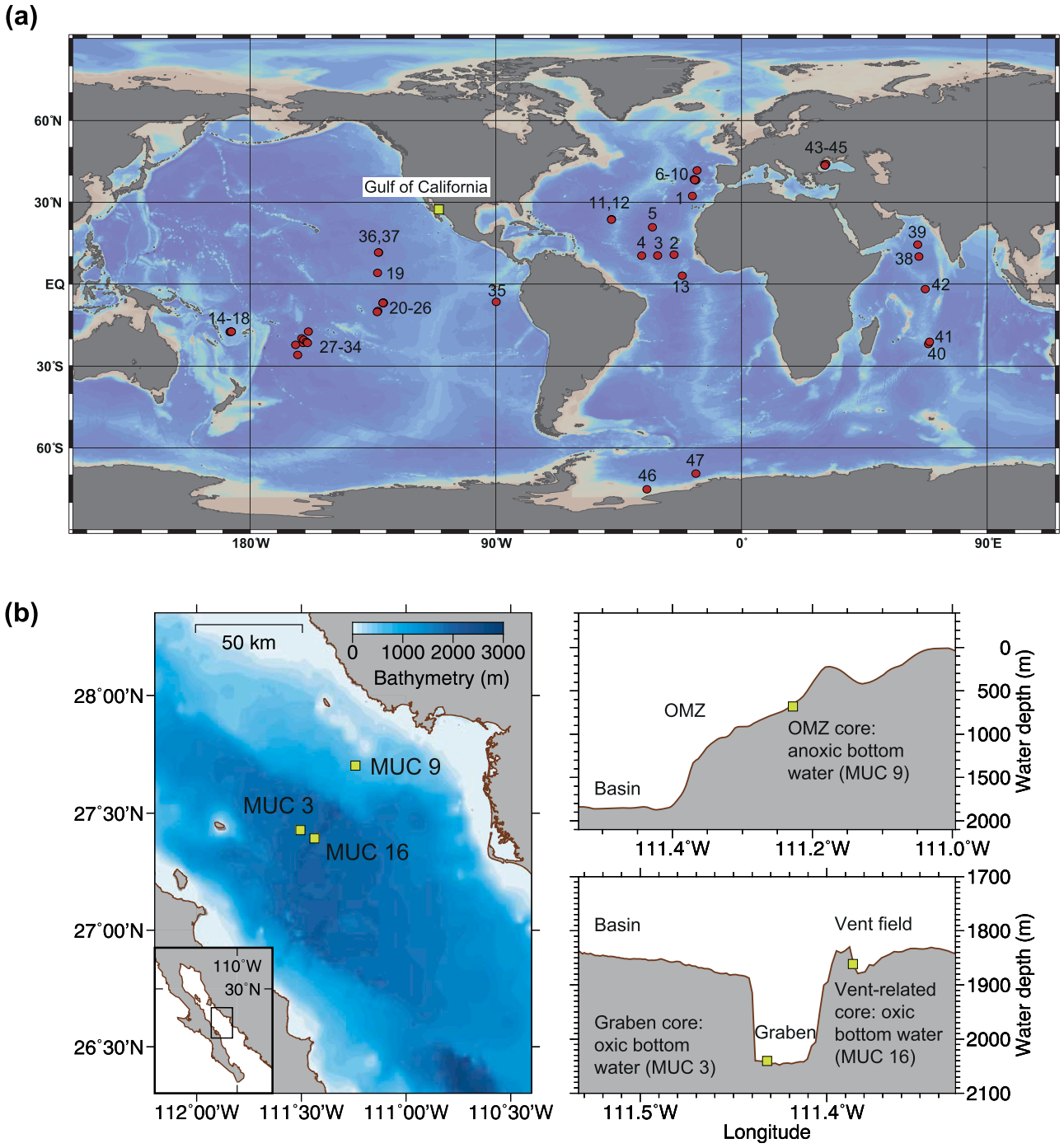

Fig. 1. (a) The locations of sediment cores at the Gulf of California (yellow square) and surface sediments (red circles) analyzed in this study. The numbers correspond to indicators listed in Table 2. (b) Sample locations and depositional settings of the three cores from the Gulf of California.

2.2. Analytical methods

2.2.1. Sample digestion

Sample preparation was conducted in the clean laboratories at the University of Cologne. Approximately 50–100 mg sediment sample powders were weighed and then transferred to pre-cleaned Teflon beakers. According to the amount of W in samples, ^{180}W-^{183}W double spike was added to achieve a sample-spike ratio of 60:40. The samples were digested on a hotplate at 120 °C with a 3:1 mixture of distilled concentrated HF and HNO_3. After at least 48 h, samples were dried down and redissolved with 4 mL concentrated HNO_3 for another 48 h. Subsequently, the samples were dissolved with 4 mL concentrated HCl. The last two steps were repeated until all the samples were clearly dissolved. Finally, the samples were dried down and redissolved in 1 M HCl for chemical separation.

2.2.2. Major and trace element analysis

Major elements in all surface ocean sediments were measured using inductively coupled plasma optical emission spectroscopy (ICP-OES, Agilent Technologies 720-ES) at the University of Cologne. Trace element concentrations were determined using a quadrupole inductively coupled plasma mass spectrometer (ICP-MS) (Agilent 7500x) at GEOMAR in Kiel. Two distinct standard calibrations were utilized to cover samples with high and low trace element concentrations, with

reproducibility being highly dependent on each specific element. Total organic carbon (TOC) contents were measured using a Dimatoc analyzer at the University of Cologne.

2.2.3. Chemical separation of W and isotopic measurement

This study employed a double spike technique (Kurzweil et al., 2018) to accurately and precisely correct for any mass-dependent isotope fractionation occurring through sample preparation, chemical separation and measurement processes. For the ^{180}W-^{183}W spike mixture used in our study, it is critical to remove Hf to avoid interference of ^{180}Hf on ^{180}W; similar precautions are necessary for Ta, because such isobaric interferences cannot be corrected by double spike. Therefore, a three-step column chemistry procedure was implemented for W separation, following the established protocol outlined in Kurzweil et al. (2018). This W separation procedure involves a BioRad AG 50 W-X8 cation exchange resin (15 mL), loading and collecting with 1 M HCl-1 % H_2O_2, followed by an anion resin AG 1 × 8 (2 mL), rinsed with the same solution and collected with 3 M HNO_3- 0.2 M HF. The final column is filled with 1 mL Eichrom TEVA to further separate W from other elements such as Ti, Zr, Hf and Mo. Elemental yields for all samples were 60–80 %. The total procedural blanks for W varied between 34 and 95 pg and were routinely monitored by doping double spike to blanks with each batch of samples. These blanks were then calculated using the double-spike inversion as applied to all samples. They correspond to 1~3 ‰ of the amount of W in the processed samples, which were negligible given the small natural variability.

Isotopic analysis of W was conducted on a Thermo Fisher Scientific Neptune Multi-collector ICP-MS at the University of Cologne. A jet sampler cone and X skimmer cone were used. The electronic baseline and gain calibrations were performed at the start of each analytical session. Isotopes ^{177}Hf, ^{178}Hf, ^{180}W, ^{181}Ta, ^{182}W, ^{183}W, ^{184}W, ^{186}W, and ^{188}Os were measured on Faraday cups equipped with 10^{11} Ω resistor amplifiers. The reference material OU-6 was measured along with samples in each batch to ensure accuracy and precision. Over a 14-month time period, OU-6 yielded values of 0.082 ± 0.021 ‰ (2SD, N = 18), consistent with previously published results at 0.080 ± 0.024 ‰ (2SD, N = 12) (Roué et al., 2021). In addition to OU-6, the pure W reference solution Alfa Aesar were measured frequently during each measurement sequence to monitor the instrument performance. The Alfa Aesar yielded values of 0.053 ± 0.007 ‰ (2SD, N = 18).

Enrichment factors for elements (X = W, Mn, or Mo) are calculated by

$$X_{EF} = \frac{(X/Al)_{bulk}}{(X/Al)_{UCC}} \quad (1)$$

Authigenic concentrations of elements (X = W, Mn and Fe) are calculated by

$$X_{auth} = X_{bulk} - Al_{bulk} \times \frac{X_{UCC}}{Al_{UCC}} \quad (2)$$

The authigenic $\delta^{186/184}$W values are calculated from the authigenic fraction following

$$\delta^{186/184}W_{auth} = \frac{\delta^{186/184}W_{bulk} - \left(\left(1 - \frac{W_{auth}}{W_{bulk}}\right) \times \left(\delta^{186/184}W_{UCC}\right)\right)}{\frac{W_{auth}}{W_{bulk}}} \quad (3)$$

Upper continental crust (UCC) values for all elements were from Rudnick and Gao (2014). The $\delta^{186/184}W_{UCC}$ has been determined at 0.043 ± 0.046 ‰ (2SD) based on glacial diamictites deposited between the Mesoarchean and the Paleozoic (Mazza et al., 2024), including modern eolian loess sourced from the vast crustal surface in China (0.01 ± 0.01 ‰ (2SE), Yang et al., 2022).

Notably, calculations reveal that the W_{EF} values of sediments in the Gulf of California are not significantly greater than 1, whereas global sediments display substantial variability, with an average W_{EF} value of 23 ± 140 (2SD, N = 37). Consequently, determining authigenic $\delta^{186/184}$W values introduces considerable uncertainties, undermining the accuracy and precision of such calculations, particularly for samples with lower W_{EF} values. Moreover, the detrital components of global sediments are unlikely to be uniform, further complicating sample comparisons based on authigenic $\delta^{186/184}$W values. Therefore, in our subsequent discussion, we focus on bulk $\delta^{186/184}$W values rather than calculated authigenic $\delta^{186/184}$W values when examining W isotopic behaviors across different sediments. The average authigenic $\delta^{186/184}$W values are used solely to estimate the average $\delta^{186/184}$W end-member of the global W sink.

3. Results

3.1. Three sediment cores from the Gulf of California, Guaymas Basin

In the investigation of W concentrations and isotope compositions across the three sediment cores from the Guaymas Basin in the Gulf of California, distinct patterns emerge related to different geological settings (Fig. 2). The highest W concentration is found in the OMZ core, averaging 1.22 ± 0.26 ppm (2SD, N = 17), followed by the graben core with 0.89 ± 0.89 ppm (2SD, N = 15). The vent-related core exhibits the lowest W concentration at 0.37 ± 0.29 ppm (2SD, N = 12) (Fig. 2 and Table 1). Isotope analyses reveal a range of $\delta^{186/184}$W values across all three cores from –0.173 to 0.104 ‰ (2SD = 0.108 ‰, N = 44). The OMZ core (MUC9) demonstrates the highest $\delta^{186/184}$W average of 0.075 ± 0.033 ‰ (2SD, N = 17). The graben core (MUC3) records a $\delta^{186/184}$W average of 0.008 ± 0.048 ‰ (2SD, N = 15), while the vent-related core (MUC16) has the lowest average of –0.034 ± 0.097 ‰ (2SD, N = 12). Notably, when excluding the extremely lowest bottom sample, the average is –0.021 ± 0.043 ‰ (2SD, N = 11), which is still lower than the UCC value.

The W enrichment factors (W_{EF}) in the graben core sediments range from 0.8 to 2.1 and correlate with Mn enrichment factors (Mn_{EF}) (R^2 = 0.71, p = 0.000089), demonstrating variability with depth (Fig. 2). Surface sediments yield higher W contents, decreasing with depth until stabilizing below 15 cm. In contrast, below a depth of 15 cm, Mo concentrations increase coevally with an increasing extent of pyritization (proportion of reactive Fe that has been converted to pyrite). The $\delta^{186/184}$W values in this core range between –0.020 and 0.069 ‰, correlating with Mn_{EF} (R^2 = 0.64, p = 0.00035). The OMZ core indicates a distinct W behavior. Although the absolute W concentrations in OMZ sediments are the highest among the three cores, their W/Al values match the UCC value, resulting in W_{EF} values ranging between 0.9 and 1.4 (Table 1 and Fig. 2). Moreover, this core shows limited $\delta^{186/184}$W variability, from 0.048 to 0.104 ‰. The vent-related core was retrieved in proximity to a hydrothermal field. The W concentration is significantly lower in this core, especially in the deepest sample, which exhibits the highest Mo and Zn concentrations (Eroglu et al., 2020). The W_{EF} values range from 0.2 to 1.2, indicating only slight W enrichment in the uppermost 2.5 cm, with the reminder of the core being depleted in W (Table 1 and Fig. 2). Additionally, this lowermost sub-sample displays the most negative $\delta^{186/184}$W value of –0.173 ± 0.018 ‰ (Fig. 2).

3.2. Surface sediments from the global ocean basins

The $\delta^{186/184}$W compositions and W concentrations of surface sediments from different ocean basins are plotted in Fig. 3 and listed in Table 2. The overall average W concentration is 2.99 ± 6.63 ppm (2SD, N = 47). There are distinct differences in W concentrations among ocean basins. In the Pacific Ocean, the average W concentration is 4.56 ± 8.02 ppm (2SD, N = 24), whereas in the Atlantic Ocean, it averages 1.49 ± 1.74 ppm (2SD, N = 13). The Indian Ocean shows a lower average of 0.97 ± 1.14 ppm (2SD, N = 5). The Black Sea sediments show a W concentration of 1.37 ± 1.23 ppm (2SD, N = 3), while the Southern Ocean sites have concentrations of 0.52 and 1.94 ppm (N = 2). The

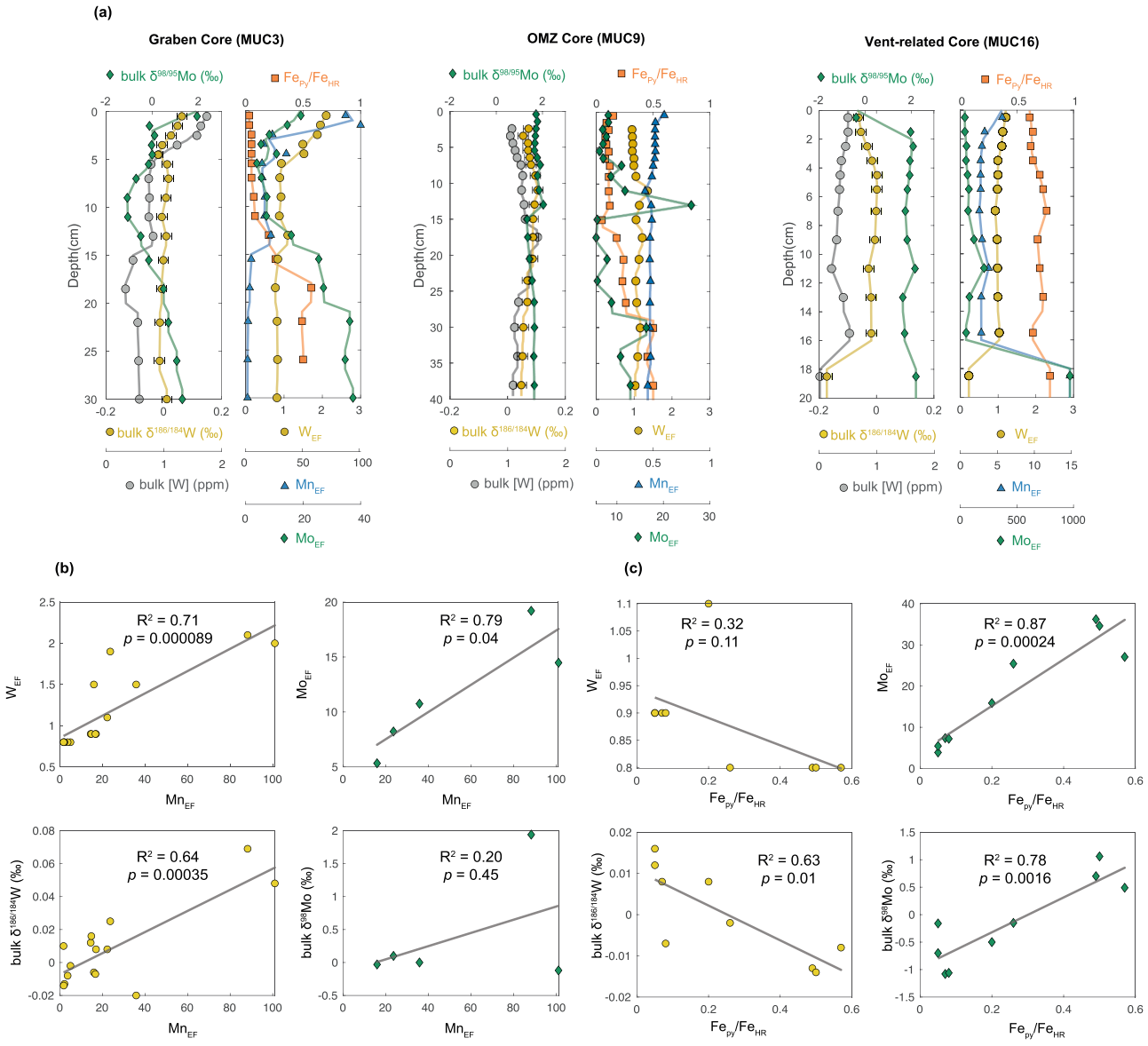

Fig. 2. (a) Geochemical profiles for sediments from three cores in the Gulf of California. The displayed data include W isotope compositions ($\delta^{186/184}W$) (yellow circles, this study), Mo isotopes ($\delta^{98/95}Mo$) (green diamonds, Eroglu et al., 2020), enrichment factors for W (W_{EF}) (yellow circles, this study), enrichment factors for Mo (Mo_{EF}) (green diamonds, Eroglu et al., 2020), and enrichment factors for Mn (Mn_{EF}) (blue triangles, Eroglu et al., 2020), as well as the ratio of pyrite-Fe to total highly reactive Fe (Fe_{Py}/Fe_{HR}) (orange squares, Eroglu et al., 2020) in sediments. (b) Correlations between enrichment factors and isotope compositions of Mo and W with Mn_{EF} in the graben core (MUC3). Mo behavior is not solely correlated with Mn, whereas W is. Since Mn change mainly occurs in the top 5 cm, W data are plotted for the whole core, while Mo data are plotted for the top 5 cm to illustrate correlations with Mn. (c) Correlations of Mo and W enrichment factors and isotope compositions with Fe_{Py}/Fe_{HR} in MUC3. To illustrate correlations with Fe_{Py}/Fe_{HR}, only data from below 5 cm are plotted, where Mn remains unchanged.

overall average $\delta^{186/184}W$ composition is 0.169 ± 0.136 ‰ (2SD, N = 47). Separately, the average $\delta^{186/184}W$ composition is highest in the sediments of the Indian Ocean and Pacific Ocean, at 0.200 ± 0.096 ‰ (2SD, $N = 5$) and 0.198 ± 0.134 ‰ (2SD, $N = 24$), respectively, followed by the sediments of the Atlantic Ocean at 0.140 ± 0.070 ‰ (2SD, N = 13). The Black Sea sediments show a $\delta^{186/184}W$ composition of 0.067 ± 0.012 ‰ (2SD, $N = 3$), while the Southern Ocean has compositions of 0.073 ‰ and 0.082 ‰ ($N = 2$). Notably, the $\delta^{186/184}W$ values in sediments from both the Black Sea and the Southern Ocean closely match the UCC value (Mazza et al., 2024). In addition, a positive relationship between the $\delta^{186/184}W$ and W_{EF} is observed for all sediments (Fig. 3b). Excluding sediments from the Black Sea, the Southern Ocean, and continental margins, the W_{EF} values in core-top samples are highly variable but generally significantly greater than 1, reaching up to 425 at a North Pacific site (See also Table 2).

4. Discussion

4.1. The diagenetic fate of W in continental margin environments

In the graben core (MUC3), W enrichments (W_{EF}) and isotopic trends ($\delta^{186/184}W$) decrease with depth, correlating with decreasing Mn enrichments (Fig. 2). The pronounced Mn_{EF} in the top few centimeters of the core originates from the precipitation of Mn oxides due to oxic bottom water conditions and re-oxidation of dissolved Mn (II) within the sediments, which diffuses upward through the pore-water along the core (Eroglu et al., 2020). Enrichment of molybdenum (Mo), tungsten's geochemical twin, also exhibit positive correlations with Mn within the upper 5 cm (Fig. 2b). Experimental studies have shown that lighter isotopes of W and Mo are preferentially adsorbed onto Mn oxides (Kashiwabara et al., 2017; Wasylenki et al., 2008). Consequently, we

Table 1
Sample depths, W concentrations and $\delta^{186/184}W$ compositions of the bulk sediments, and W enrichment factors for three cores from the Gulf of California.

Sample ID	Sediment depth (cm)	Bulk [W] (ppm)	Bulk $\delta^{186/184}W$ (‰)	W Enrichment Factor	[Mn]* (ppm)	[Fe]* (ppm)	[Al]* (ppm)
16_MUC03_2043_0.5_20	0.5	1.74	0.069	2.1	29,854	18,322	35,635
16_MUC03_2043_1.5_21	1.5	1.64	0.048	2.0	34,810	18,540	36,109
16_MUC03_2043_2.5_22	2.5	1.57	0.025	1.9	8095	18,060	36,113
16_MUC03_2043_3.5_23	3.5	1.23	−0.006	1.5	5363	18,212	35,432
16_MUC03_2043_4.5_24	4.5	0.91	−0.020	1.5	8754	14,142	25,706
16_MUC03_2043_5.5_25	5.5	0.78	0.012	0.9	4924	18,207	35,979
16_MUC03_2043_7_26	7.0	0.74	0.016	0.9	4987	18,005	35,661
16_MUC03_2043_9_27	9.0	0.75	0.008	0.9	5628	17,645	35,021
16_MUC03_2043_11_28	11.0	0.74	−0.007	0.9	5722	18,204	36,210
16_MUC03_2043_13_29	13.0	0.82	0.008	1.1	6719	16,532	31,855
16_MUC03_2043_15.5_30	15.5	0.47	−0.002	0.8	1111	11,476	23,942
16_MUC03_2043_18.5_31	18.5	0.34	−0.008	0.8	632	8047	18,679
16_MUC03_2043_22_32	22.0	0.55	−0.013	0.8	564	13,949	28,736
16_MUC03_2043_26_33	26.0	0.56	−0.014	0.8	473	14,005	29,102
16_MUC03_2043_30_34	30.0	0.58	0.010	0.8	473	14,684	30,314
29_MUC09_667_2.5_3	2.5	1.08	0.073	0.9	241	22,849	48,928
29_MUC09_667_3.5_4	3.5	1.05	0.054	1.0	232	22,748	47,220
29_MUC09_667_4.5_5	4.5	1.09	0.071	1.0	239	23,294	48,617
29_MUC09_667_5.5_6	5.5	1.13	0.072	1.0	253	24,327	51,098
29_MUC09_667_6.5_7	6.5	1.17	0.077	1.0	246	23,801	50,378
29_MUC09_667_7.5_8	7.5	1.23	0.082	1.0	254	25,020	53,390
29_MUC09_667_9_9	9.0	1.26	0.097	1.0	241	23,876	51,753
29_MUC09_667_11_10	11.0	1.24	0.104	1.4	161	16,586	39,452
29_MUC09_667_13_11	13.0	1.29	0.094	1.1	223	21,999	48,584
29_MUC09_667_15_12	15.0	1.30	0.088	1.1	248	24,190	53,283
29_MUC09_667_17.5_13	17.5	1.52	0.088	1.2	242	24,476	53,846
29_MUC09_667_20.5_14	20.5	1.40	0.087	1.1	239	24,556	53,302
29_MUC09_667_23.5_15	23.5	1.36	0.069	1.0	255	25,338	56,136
29_MUC09_667_26.5_16	26.5	1.19	0.069	1.1	215	21,562	47,839
29_MUC09_667_30_17	30.0	1.12	0.055	1.2	187	21,340	41,537
29_MUC09_667_34_18	34.0	1.17	0.052	1.1	209	21,394	45,934
29_MUC09_667_38_19	38.0	1.10	0.048	1.0	198	20,193	45,822
66_MUC16_1853_0.5_35	0.5	0.50	−0.062	1.2	962	244,900	17,900
66_MUC16_1853_1.5_36	1.5	0.50	−0.054	1.1	602	244,400	19,300
66_MUC16_1853_2.5_37	2.5	0.46	−0.032	1.1	499	297,900	18,000
66_MUC16_1853_3.5_38	3.5	0.39	−0.015	1.0	434	213,600	16,700
66_MUC16_1853_4.5_39	4.5	0.37	0.002	1.0	410	215,900	15,800
66_MUC16_1853_5.5_40	5.5	0.35	0.001	1.0	405	221,400	15,500
66_MUC16_1853_7_41	7.0	0.33	−0.001	0.9	370	227,200	15,200
66_MUC16_1853_9_42	9.0	0.30	−0.005	1.0	373	237,400	13,400
66_MUC16_1853_11_43	11.0	0.22	−0.028	1.0	341	259,800	9400
66_MUC16_1853_13_44	13.0	0.42	−0.019	1.0	487	222,100	18,200
66_MUC16_1853_15.5_45	15.5	0.53	−0.018	1.0	591	176,900	22,000
66_MUC16_1853_18.5_46	18.5	0.014	−0.173	0.2	380	277,000	2700

* The Mn, Fe and Al concentration data are from Eroglu et al. (2020).

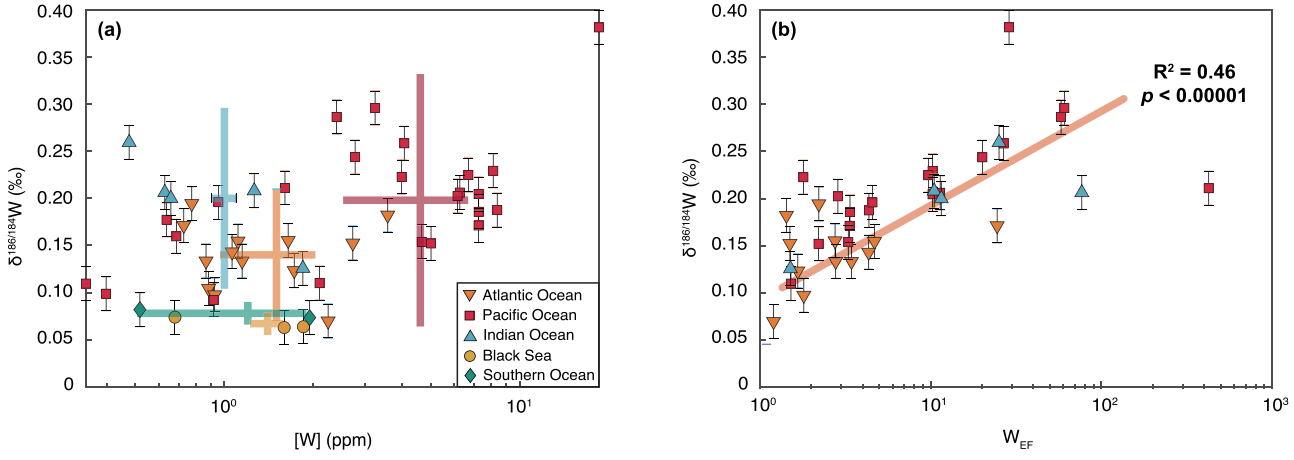

Fig. 3. Scatter plots of bulk $\delta^{186/184}W$ against bulk W concentrations and W_{EF} for open ocean sediments measured in this study. Each point represents a sample, with different symbols indicating ocean basins (as shown in the legend). The thick error bars denote the 2SD errors for each category of sediments, with colors corresponding to the legend.

Table 2
Sample information, W concentrations and $\delta^{186/184}W$ compositions of the bulk sediments, major element concentrations and total organic carbon (TOC) contents for surface sediments from different ocean basins investigated in this study.

Sample IDs	Latitude	Longitude	Location	Depth (m)	Bulk [W] (ppm)	Bulk $\delta^{186/184}W$ (‰)	W Enrichment Factor	[Mn] (ppm)	[Fe] (ppm)	[Al] (ppm)	TOC (%)	Map
M19_10,743	32.23	−18.29	Canary Basin	4486	0.73	0.171	24.5	140	16,113	1275	0.31	1
SO237_2–2 GC1	10.72	−25.06	Cape Verde Basin	5463	0.88	0.104	0.9	575	23,721	40,775	0.30	2
SO237_4–10 GC3	10.41	−31.09	Cape Verde Basin	5823	3.57	0.182	1.4	483	69,033	107,143	0.44	3
SO237_6–6 GC4	10.35	−36.96	Cape Verde Basin	5135	2.72	0.152	1.5	6852	50,127	77,890	0.23	4
M60/*A* + *B*_16,036–1	20.77	−33.01	Cape Verde Basin	5170	1.72	0.123	1.7	1278	25,864	44,364	0.50	5
MSM96_36_MUC_liner4	38.16	−17.51	Iberian Basin	5333	1.11	0.155	4.7	1262	19,667	10,173	0.30	6
MSM96_57_MUC_liner3	41.59	−16.60	Iberian Basin	5497	2.24	0.070	1.2	1225	48,423	80,088	0.38	7
MSM96_51_MUC_liner2	38.00	−17.06	Iberian Basin	5556	1.64	0.155	2.8	1964	29,807	25,594	0.46	8
MSM96_55_MUC_liner4	38.40	−17.69	Iberian Basin	5476	1.15	0.133	3.4	1096	20,055	14,338	0.35	9
MSM96_37_MUC_liner7	38.09	−17.45	Iberian Basin	5210	1.06	0.143	4.3	1042	16,350	10,506	0.20	10
M139_961	23.72	−48.06	Mid-Atlantic Ridge	4166	0.93	0.098	1.8	1764	17,198	22,013	0.11	11
M139_960	23.55	−48.09	Mid-Atlantic Ridge	4251	0.87	0.133	2.8	1426	12,877	13,384	0.14	12
M51_13,520–1	3.02	−22.03	Sierra Leone Basin	4500	0.78	0.194	2.2	881	10,321	15,034	0.48	13
SO99_67	−17.00	173.63	near Fiji Plateau	3150	0.40	0.099	0.6	462	19,810	29,162	0.15	14
SO134–46	−17.10	173.32	near Fiji Plateau	3028	0.64	0.177	0.6	4054	66,857	48,429	0.16	15
SO134–59	−17.00	173.84	near Fiji Plateau	2385	0.69	0.160	0.8	4591	61,360	38,621	0.30	16
SO134–107	−17.00	173.83	near Fiji Plateau	2407	0.92	0.092	0.9	2942	57,407	46,408	0.10	17
SO134–108	−17.00	173.86	near Fiji Plateau	2082	0.34	0.110	0.2	1704	115,959	77,745	0.08	18
SO06/1_34	4.05	−134.11	Central Pacific Basin	4570	3.23	0.296	60.7	3959	11,016	2287	0.07	19
SO06/1_47	−7.00	−132.02	Central Pacific Basin	4682	4.06	0.258	26.8	5596	17,078	6510	0.52	20
SO06/1_51	−6.99	−132.16	Central Pacific Basin	4913	8.12	0.229	10.3	13,660	44,007	33,940	0.29	21
SO06/1_79	−6.82	−132.02	Central Pacific Basin	4769	6.26	0.206	11.4	9310	30,194	23,613	0.34	22
SO06/1_92	−7.00	−131.93	Central Pacific Basin	4529	2.40	0.286	58.1	2683	9877	1770	0.18	23
SO06/1_96	−6.98	−132.13	Central Pacific Basin	4887	7.24	0.205	10.3	13,025	38,970	30,304	0.18	24
SO06/1_124	−9.92	−134.00	Taki Basin	4387	2.77	0.244	20.1	7214	28,109	5914	0.00	25
SO06/1_148	−10.27	−134.25	Taki Basin	4687	6.69	0.225	9.7	21,564	82,860	29,609	0.15	26
SO06/2_214	−21.59	−161.54	Aguila Fracture Zone	4463	4.65	0.154	3.3	8449	96,910	60,637	0.19	27
SO06/2_233	−26.01	−163.49	Aguila Fracture Zone	5200	6.15	0.202	2.9	11,876	88,591	92,171	0.23	28
SO06/2_162	−17.45	−159.56	Aguila Fracture Zone	5232	8.38	0.188	4.4	18,934	108,050	82,637	0.35	29
SO06/2_184	−19.95	−162.00	Aguila Fracture Zone	5006	7.25	0.186	3.4	13,417	100,346	92,315	0.25	30
SO06/2_198	−20.48	−161.25	Aguila Fracture Zone	5200	7.24	0.171	3.3	14,845	113,461	92,784	0.27	31
SO06/2_200	−21.21	−160.29	Aguila Fracture Zone	4697	5.00	0.152	2.2	9844	145,045	97,350	0.29	32
SO06/2_206	−21.60	−159.88	Aguila Fracture Zone	4286	2.10	0.110	1.5	2955	104,120	59,263	0.30	33
SO06/2_236	−22.32	−164.25	Aguila Fracture Zone	5200	3.98	0.223	1.8	6630	91,862	94,984	0.41	34
SO106_292	−6.57	−90.47	Peru Basin	4127	18.49	0.381	28.8	96,134	27,900	27,557	0.46	35

(*continued on next page*)

Table 2 (*continued*)

Sample IDs	Latitude	Longitude	Location	Depth (m)	Bulk [W] (ppm)	Bulk $\delta^{186/184}$W (‰)	W Enrichment Factor	[Mn] (ppm)	[Fe] (ppm)	[Al] (ppm)	TOC (%)	Map
SO06/1_04	11.51	−133.71	North Pacific Basin	4916	1.60	0.211	425.3	3203	11,600	162	0.03	36
SO06/1_05	11.53	−133.79	North Pacific Basin	4774	0.95	0.196	4.6	1599	9987	8974	-	37
SO118_1	10.03	65.00	Arabian Basin	4425	1.84	0.126	1.5	1255	40,416	52,381	0.36	38
SO118_3	14.42	64.57	Arabian Basin	3955	1.26	0.208	10.5	1281	16,754	5161	0.31	39
SO28_00044	−22.01	68.52	Mid-Indian Ridge	3212	0.63	0.206	76.8	1640	12,000	351	0.21	40
SO28_00062	−21.19	68.94	Mid-Indian Ridge	2942	0.66	0.200	11.5	2042	19,838	2451	0.25	41
SO28_00018	−1.89	67.34	Mabahiss Fracture Zone	3035	0.48	0.259	25.2	336	5165	812	0.42	42
MSM34/2_22–1 GC2	43.43	30.43	Black Sea	1551	1.59	0.063	0.9	1128	44,294	72,329	0.93	43
MSM34/2_3–3 GC1	43.81	30.41	Black Sea	418	1.85	0.064	1.1	687	42,647	72,639	0.78	44
MSM34/2_89–1 GC9	43.96	30.80	Black Sea	824	0.68	0.074	0.9	216	17,517	33,274	1.40	45
PS111_80–3	−76.39	−35.26	Weddell Sea	932	1.94	0.073	0.9	714	63,027	97,297	1.03	46
PS111_16–3	−71.23	−17.49	Weddell Sea	1418	0.52	0.082	0.3	739	61,365	64,220	0.42	47

would expect the W and Mo isotopes of sediments to become heavier with increasing depth, as lighter isotopes are released during the dissolution of Mn oxides, rendering the residual bulk sediment W and Mo isotope signals heavier. However, the observed opposite trend in solid phases, along with pore-water Mo isotopic data, suggests that Mo diffuses upward and precipitates following Mn oxide dissolution (Eroglu et al., 2020). Pore-water Mo appears to be entirely governed by the solid phase, which represents a much larger Mo reservoir. Additionally, exchange between subsurface sediments and bottom seawater is unlikely, as the gradient probably drives diffusion from pore-water to bottom seawater. We therefore propose that continuous exchange between pore-water and the remaining solid phase may be a primary factor, which could also explain the W isotopic trend. Below 5 cm, variations in $\delta^{98/95}$Mo values and Mo_{EF} correlate with a simultaneous increase in Fe_{Py} in the solid phase, which is not the case for $\delta^{186/184}$W or W_{EF} (Fig. 2c). Notably, around the transition boundary between 13–15 cm, a slight decrease in Mn alongside a significant increase in Fe appears to coincide only with a decrease in W concentration, with no detectable W isotopic fractionation (Fig. 2a). This could be explained by the quantitative release of labile W from the solid phase into the pore-water without isotopic fractionation, supported by the lack of authigenic W enrichment at these sedimentary depths. As a result, $\delta^{186/184}$W stabilizes at 0.001 ± 0.022 ‰ (2SD). This stabilization strikingly matches the average crustal (detrital) W isotopic composition (0.043 ± 0.046 ‰, Mazza et al., 2024).

In the OMZ core (MUC9), which is characterized by more reducing conditions, lower Mn and higher Fe contents in sediments (Eroglu et al., 2020), W and Mo behave differently, with W showing less variability compared to the Mn-dominated graben core. The limited Mn presence in the OMZ core, as reported by Scholz et al. (2019) and Eroglu et al. (2020), is attributed to the high mobility of Mn in the anoxic water column and surface sediments. Reductive Mn dissolution in the surface sediment releases dissolved Mn into the pore-waters, which is transported across the sediment-bottom water interface via diffusion. Due to anoxic conditions in the bottom water and slow Mn oxidation kinetics, Mn is transported laterally and the sediments left behind are thus depleted in Mn. Below a sediment depth of 19 cm, where sulfidic conditions prevail, Mo_{EF} slightly increases. However, W_{EF} remains constant around the detrital value throughout the OMZ core. Experimental studies (Cui et al., 2021) indicate that Mo's higher degree of thiolation results in efficient removal from the dissolved phase under sulfidic conditions. Conversely, dissolved W concentrations increase under sulfidic conditions, as its oxyanion-to-thiolated phase transition requires higher sulfide concentrations than Mo. In addition, thiolated W species have a lower affinity for reactive surfaces compared to Mo (Mohajerin et al., 2016). Throughout the OMZ core, $\delta^{186/184}$W values also show minor variations (Fig. 2). Due to the low Mn contents, little authigenic W is present throughout the core, making sedimentary W predominantly detrital-like, as observed in the lower section of the graben core.

In sediments influenced by hydrothermal activities (MUC16), W behavior differs from other elements such as Mo, Zn and Fe (Eroglu et al., 2020), suggesting unique geochemical processes. Although Fe is highly enriched in the vent-related core and the Fe_{Py}/Fe_{HR} ratio surpasses that of the other two cores, W concentrations are not significantly enriched compared to the UCC (Fig. 2 and Table S1). The inverse relationship between W_{EF} and Fe_{Py}/Fe_{HR} (Fig. 2) further supports our findings from the graben core, which suggest that W is not incorporated into sedimentary pyrite or other sulfide minerals. Rather, W appears to be depleted in pyrite-rich samples. Regarding the $\delta^{186/184}$W values in the sediments, the average $\delta^{186/184}$W for the vent-related core is comparable to that of the graben core MUC3, at around –0.021 ± 0.043 ‰, slightly lower than UCC composition. The lighter isotopic signature of W in these two cores compared to the OMZ core could result from existence of authigenic Mn oxides under conditions of slight oxygenation, which leads to the adsorption of the lighter W isotopes. Notably, the lowermost sample of the vent-related core is an anomaly, characterized by low W content but elevated Mo and Fe_{Py}/Fe_{HR} (Fig. 2). Previous studies have shown that this vent-related core comprises a mixture of black smoker chimney debris and hemipelagic sediment (Eroglu et al., 2020). The strong correlation observed between Zn and Mo likely reflects their co-precipitation with Fe minerals within vent edifices under highly reducing fluid conditions (Berndt et al., 2016). Consequently, the Fe minerals in the lower samples, particularly the bottom sample, are unlikely to serve as sufficient sorbents for W in reducing hydrothermal environments. Additionally, W is not extraordinarily enriched in hydrothermally derived Fe-Mn crusts compared to hydrogenetic Fe-Mn crusts formed from seawater in the deep Pacific Ocean (Yang et al., 2023). To better understand the role of hydrothermal circulation in the marine W cycle, additional investigations into hydrothermal systems at mid-ocean ridges and flanks are essential.

4.2. W burial in global ocean basins

Sediments in the Gulf of California cover the range of redox

conditions that is typical for continental margins. Oxic surface sediments are characterized by Mn and W enrichments. However, upon Mn reduction, W seems to be released and authigenic W burial under more reducing conditions is limited in all downcore records investigated. Our study of W cycling in the graben core suggests that loss of Mn, and consequently W, across the sediment-water interface is not expected under fully oxic conditions. Therefore, oxic core-top (surface) sediments from multiple ocean basins—including the Pacific, Atlantic, Indian, and the Southern Oceans —were analyzed to investigate W burial in the global ocean.

The oxic surface sediments in global ocean basins indicate significant authigenic W enrichments, and the bulk $\delta^{186/184}$W values of the sediments (0.169 ± 0.020 ‰, 2SE, N = 47), as well as the calculated authigenic $\delta^{186/184}$W values of the sediments (0.255 ± 0.025 ‰, 2SE, N = 37), both fall between the compositions of seawater (0.543 ± 0.046 ‰ (Fujiwara et al., 2020; Kurzweil et al., 2021)) and Fe-Mn crusts (−0.04 ‰ ± 0.02 ‰ (Yang et al., 2023)) (Fig. 3). Notably, higher authigenic W contents, indicated by higher W_{EF}, correspond to heavier $\delta^{186/184}$W signatures (Fig. 3b). $\delta^{186/184}$W compositions of Black Sea sediments are close to UCC compositions and show no authigenic enrichment of W (Fig. 3a). This is also consistent with selected Black Sea samples reported previously (Roué et al., 2021) and confirms that W cannot be enriched under euxinic conditions. In a similar fashion, the two sediment samples from the Southern Ocean display UCC-like W concentrations and $\delta^{186/184}$W values (Fig. 3).

Since modern seawater is reported to have a homogenous $\delta^{186/184}$W composition and because W is conservative throughout salinity-normalized seawater depth profiles without biological influences (Fujiwara et al., 2020; Kurzweil et al., 2021), we can assume that authigenic W in surface sediments in the global open ocean is deposited from bottom seawater with identical $\delta^{186/184}$W compositions. Marine sediments exhibit a wide variety of compositions, including Fe-Mn oxides, terrigenous or authigenic clay minerals, carbonates, detrital silicates, and organic matter. Fe-Mn oxides, clay minerals and organic material have been identified as potential host phases for W, with Fe-Mn oxides exhibiting significantly higher adsorption capacity, particularly under seawater pH conditions (Iwai and Hashimoto, 2017; Kashiwabara et al., 2017; Sen Tuna and Braida, 2014). However, the extent to which other phases incorporate W and contribute to isotopic fractionation during these processes remains unclear and requires further investigation. Authigenic W concentrations are plotted against authigenic Mn, Fe concentrations and total organic carbon (TOC) contents in Fig. 4. The most notable correlation was found between authigenic W and authigenic Mn across all sediment samples. Pacific sediments exhibit the highest levels of authigenic W and Mn (Fig. 4a). Large areas of Mn nodules in the Pacific have been reported (Hein et al., 1997). The correlation between authigenic W and Fe is not as pronounced as the one between W and Mn (Fig. 4b). No positive correlation between authigenic W and TOC is observed for all sediments (Fig. 4c). Based on the strong correlation between authigenic W and authigenic Mn in our dataset, along with experimental results (Kashiwabara et al., 2017), it is evident that authigenic Mn oxide phases effectively scavenge dissolved W from the water, acting as a major W sink. However, results from adsorption experiments of W onto Fe-Mn oxides show an isotopic fractionation of 0.50 ± 0.06 ‰ for ferrihydrite and 0.58 ± 0.14 ‰ for δ-MnO_2 under equilibrium conditions (Kashiwabara et al., 2017). Thus, the equilibrium isotope fractionation that occurs during adsorption of W onto Mn oxides is supposed to be higher than what we observed. Similar to the graben site, isotopically heavy W appears to be concentrated at the sediment surface, possibly through processes such as continuous exchange between pore-water and the solid phase, where pore-water carrying W diffuses upward and preferentially heavy W isotopes are re-adsorbed onto Mn oxides. A similar sequence of processes could explain the shift towards isotopically heavier W observed in surface sediment compilations compared to experimental data. Additionally, although reductive re-dissolution and isotopic exchange may occur at the sediments-water interface, they are unlikely to be the primary drivers of the heavier W isotope compositions observed under oxic conditions in deep-ocean surface sediments.

It is clear that W isotope fractionation between seawater and sediments differs from that observed between seawater and Fe-Mn crusts (Yang et al., 2023). In this context, it should be emphasized that over thirty different Mn oxide and hydroxide minerals are abundantly distributed across various geological settings (Post, 1999), with likely variable isotopic fractionation factors controlling the differences between these phases. Sediments also contain different types of Fe and Mn oxides, including higher concentrations of hematite and magnetite compared to Fe-Mn crusts, as well as various Mn (III) and Mn (IV) oxides formed during diagenesis. Even with a single Mn mineral like birnessite, studies on Tl isotopes, which exhibit a strong correlation with Mn oxides in modern oceans comparable to that of W, have shown that the proportion of hexagonal birnessite influences the extent of Tl enrichment and isotopic fractionation (Peacock and Moon, 2012). Similar complexities could also be speculated to affect elements like W. In addition, during oxic sedimentary diagenesis and under mild hydrothermal conditions, the nucleation and growth of Mn oxides, such as the transformation from birnessite to todorokite, can release trace elements (Atkins et al., 2014), leading to isotopic fractionation. For instance, the trace metal Ni has been observed to be released into marine pore-water during oxic diagenesis (Atkins et al., 2016). As todorokite is commonly believed to form through the transformation of birnessite, it may represent the ultimate stable Mn mineral in environments where pore-waters become sufficiently oxidizing for dissolved Mn to re-precipitate near the sediment-water interface. Light W isotopes may be released during recrystallization under oxic conditions, potentially returning to the bottom water, while the heavier W isotopes remain in the authigenic phases within surface sediments.

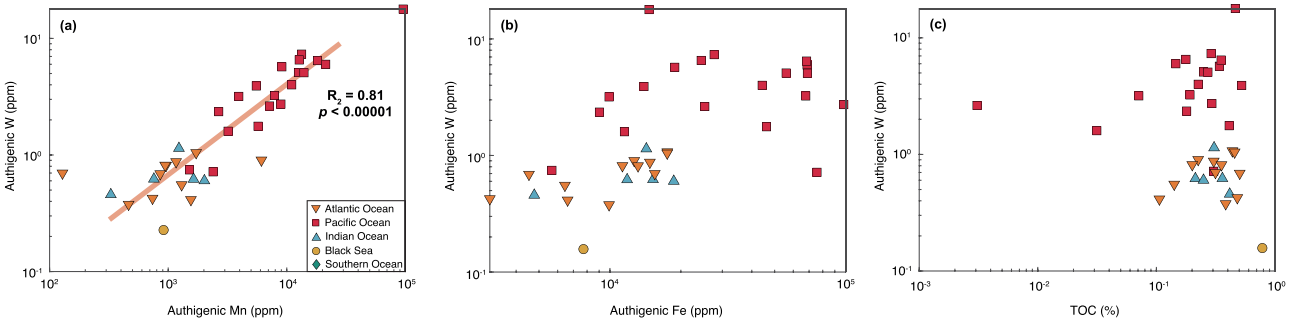

Fig. 4. Scatter plots of calculated authigenic W concentrations vs authigenic Mn (a), authigenic Fe (b), total organic carbon (TOC) (c) for surface sediments from different ocean basins. Authigenic concentrations for W, Mn, and Fe are calculated from UCC values (Rudnick and Gao, 2014) to remove the detrital components.

4.3. W mass balance in the modern ocean

Tungsten burial in the ocean is predominantly associated with Mn oxides, which are present in various forms on the ocean floor, including Mn crusts/nodules and micro-Mn oxide particles in sediments. A global net output flux of Mn in oxic sediments was estimated at up to 1.1×10^{11} mol/yr (van Hulten et al., 2017). To estimate W burial linked to total Mn oxides in sediments, an authigenic W/Mn ratio of 2.01×10^{-4} mol/mol can be obtained from our global surface sediment data (Fig. 2a), excluding sediments lacking authigenic W or Mn accumulations. This yields an estimated W burial flux of up to 22.2×10^6 mol/yr associated with total Mn oxides. In Mn crusts, W concentrations typically range from 42 to 134 ppm, averaging 65 ppm. Studies have estimated the mass flux of Mn crusts and nodules to be 0.025 g/m^2 per year (Kraemer and Schornick, 1974). By combining the area of pelagic accumulation, which is 3×10^8 km^2, the W burial flux in Mn crusts and nodules is calculated to be 2.6×10^6 mol/yr. Therefore, beyond the Mn crusts and nodules, the dispersed Mn oxides in pelagic sediments account for an additional W burial flux of 19.6×10^6 mol/yr. This value is consistent with an earlier estimate by Yang et al. (2022), who calculated W burial based on the W/Mo ratio of non-euxinic sediments and a better constrained Mo burial flux. However, our updated estimate suggests that the W burial flux (possibly Mo burial as well) in Mn oxides may be higher than previously thought. The $\delta^{186/184}$W end member of authigenic W in bulk oxic sediments can be determined using the average value of 0.255 ± 0.025 ‰ (2SE, $N = 37$) obtained from global surface sediments, excluding samples with detrital sources (Table S1).

Therefore, the output of W connected to Mn oxides is already at the same level as and even higher than major input of rivers, at ~17×10^6 mol/yr, with a $\delta^{186/184}$W value estimated at 0.37 ± 0.04 ‰ (2SE, $N = 35$) (Yang et al., 2022) (Table 3). Assuming the modern ocean is at a steady state, and based on the elemental mass and isotopic balance:

$$Flux_{input} = Flux_{output} \tag{4}$$

$$Flux_{input} \times \delta^{\frac{186}{184}}W_{input} = Flux_{output} \times \delta^{\frac{186}{184}}W_{output} \tag{5}$$

There need to be more isotopically light W inputs to the ocean to maintain the W mass and isotopic balance. The re-dissolution of W at the seafloor might be a substantial additional benthic flux to the ocean. Research on the W isotope system is still in its early stages, and many uncertainties remain regarding the marine W budget. For example, riverine inputs might be biased due to insufficient global measurements of river waters, necessitating further studies. Additionally, the magnitude of the benthic W fluxes from shelf environments was estimated based on Fe by using the total input of dissolved Fe from continental shelf sediments to the ocean and an average W/Fe ratio for reductively extracted Fe-Mn oxides of terrestrial sediments (Yang et al., 2022). However, our updated findings indicate that Mn is more closely associated with W compared to Fe. Since Mn is more readily recycled to the bottom water compared to Fe, marine sediments could be an additional source of benthic W fluxes, suggesting that the benthic W flux has likely been underestimated. Additionally, W outputs with heavier $\delta^{186/184}$W compositions to the ocean might also be a solution for the oceanic W isotopic mass balance. The selective enrichment of W compared to the more immobile elements U, Th, Ta, and Hf across altered oceanic crust has been reported (Reifenröther et al., 2022, 2021), though the low absolute W concentrations in altered oceanic crust suggest a minimal possibility of being a significant sink for W in the ocean.

Table 3
Input and output fluxes of W ($\times 10^6$ mol/yr) and W isotopes ($\delta^{186/184}$W, ‰) in the modern ocean.

	Input fluxes ($\times 10^6$ mol/yr)	$\delta^{186/184}$W (‰)	Reference
Rivers	17	0.37 ± 0.04 ‰	(Yang et al., 2022)
Benthic reflux	1.1	0.01*	(Yang et al., 2022)
Hydrothermal	<0.4	0.09*	(Yang et al., 2022)
	Output fluxes ($\times 10^6$ mol/yr)		
Oxic sediments	22.2		This study
Fe-Mn crusts/ nodules	2.6	–0.04 ± 0.02 ‰	(Yang et al., 2022) and this study
Mn oxides in sediments	19.6	0.255 ± 0.025 ‰	This study
Euxinic sediments	<0.4	0.067 ± 0.012 ‰	(Yang et al., 2022) and this study
Hydrothermal	<0.9	0.54*	(Yang et al., 2022)

*Values are calculated using indirect estimations.

4.4. Summary and implications

In this study, we investigated W cycling in three sediment cores from the Gulf of California and a global dataset of surface sediments from well-oxygenated deep-sea environments. Our findings indicate that sediment cores from the Gulf of California, which encompass various redox environments ranging from manganous to sulfidic, predominantly contain detrital W with minimal burial of authigenic W. Notably, a hydrothermal vent-related core exhibited the strongest depletion of W. This observation suggests that neither typical continental margin sediments nor hydrothermal deposits act as a major sink for W. Tungsten cycling in shallow sediments is generally coupled with Mn cycling. Under anoxic conditions, Mn oxides undergo reductive dissolution and W is lost from the solid phase so that there is no W burial. In contrast, oxic and Mn-rich surface sediments in oxygenated deep-sea regions are identified as the most significant sink for W, with a flux of 19.6×10^6 mol/yr, and an average isotopic endmember for authigenic W at 0.255 ± 0.025 ‰.

Traditionally, Mn enrichment in ancient sedimentary layers is considered a marker of Earth's oxygenation. One crucial indicator of rising atmospheric oxygen is the oxidation of Mn in the water column, which requires the presence of free oxygen. Due to the lack of correlations between W and other elements or TOC values in global marine sediments, aside from Mn, this study proposes that, to our current knowledge, no processes other than those related to Mn cycling influence the behavior of W and its isotopes in the ocean. This is unlike other metal stable isotope systems such as Mo and Ni, which are influenced by processes involving Mn oxides, as well as sulfide minerals and organic matters in euxinic environments (Fleischmann et al., 2023; Kendall et al., 2017). Mn has only one stable isotope, ^{55}Mn, meaning that there is no Mn-based isotopic tool to study the size of the global Mn sink as a function of deep-ocean oxygenation. As an alternative, stable W isotopes could potentially be used as a tracer to quantify Mn oxide burial in oxygenated seafloor environments in the geological past. Fe-Mn crusts have been used to study seawater W isotope evolution over tens of millions of years (Yang et al., 2023). To further develop this idea, future studies need to look for an appropriate archive recording the W isotope composition of seawater in deeper time. Additionally, more comprehensive studies on W isotopic fractionation across various Fe and Mn oxide minerals, as well as more downcore studies in authigenic W enriched pelagic core sites, would be necessary before applying this proxy system to reconstruct past seawater changes.

CRediT authorship contribution statement

Ruiyu Yang: Writing – review & editing, Writing – original draft, Visualization, Resources, Project administration, Methodology, Investigation, Funding acquisition, Formal analysis, Data curation, Conceptualization. **Marcus Gutjahr:** Writing – review & editing, Supervision, Resources, Funding acquisition, Conceptualization. **Florian Scholz:** Writing – review & editing, Resources, Conceptualization. **Florian Kurzweil:** Writing – review & editing, Funding acquisition, Conceptualization. **Sümeyya Eroglu:** Writing – review & editing. **Carsten**

Münker: Writing – review & editing, Supervision, Funding acquisition, Conceptualization.

Declaration of competing interest

All authors wish to confirm that there are no known conflicts of interest associated with this publication and there has been no significant support for this work that could have influenced its outcome.

All authors confirm that the manuscript has been read and approved by all named authors and that there are no other persons who satisfied the criteria for authorship but are not listed. All authors further confirm that the order of authors listed in the manuscript has been approved by all of the authors.

Acknowledgments

We express great thanks to Ana Kolevica at GEOMAR, as well as Jochen Scheld and Nicole Mantke at the University of Cologne, for their assistance with ICP-MS, ICP-OES and TOC analyses. Special thanks to Dr. Doris Maicher for kindly providing access to the drill cores from the GEOMAR Core Repository. Additionally, we are thankful to Dr. Sophie Paul for providing sediments from the Iberian Basin. This research was financially supported by the German Research Foundation (DFG) (Grant No KU 3788/3–1). Sample collection in the Gulf of California and part of the analyses were funded by the German Research Foundation through the Emmy Noether Nachwuchsforschergruppe ICONOX ("Iron Cycling in Continental Margin Sediments and the Nutrient and Oxygen Balance of the Ocean") and by the German Ministry of Education and Research through the MAKS project. This study used sediment samples obtained during scientific cruise PS111 onboard RV Polarstern in 2018 (Grant No AWI_PS111_00; Alfred-Wegener-Institut Helmholtz-Zentrum für Polar- und Meeresforschung, 2017).

Supplementary materials

Supplementary material associated with this article can be found, in the online version, at doi:10.1016/j.epsl.2025.119346.

Data availability

All data from this study are provided within this article and its supplementary information file.

References

Alam, M., Tripti, M., Gurumurthy, G.P., Sohrin, Y., Tsujisaka, M., Singh, A.D., Takano, S., Verma, K., 2022. Palaeoredox reconstruction in the eastern Arabian Sea since the late Miocene: insights from trace elements and stable isotopes of molybdenum (δ98/95Mo) and tungsten (δ186/184W) at IODP Site U1457 of Laxmi Basin. Palaeogeogr. Palaeoclimatol. Palaeoecol 587, 110790.

Atkins, A.L., Shaw, S., Peacock, C.L., 2014. Nucleation and growth of todorokite from birnessite: implications for trace-metal cycling in marine sediments. Geochim. Cosmochim. Acta 144, 109–125.

Atkins, A.L., Shaw, S., Peacock, C.L., 2016. Release of Ni from birnessite during transformation of birnessite to todorokite: implications for Ni cycling in marine sediments. Geochim. Cosmochim. Acta 189, 158–183.

Barron, J.A., Bukry, D., Bischoff, J.L., 2004. High resolution paleoceanography of the Guaymas Basin, Gulf of California, during the past 15 000 years. Mar. Micropaleontol. 50, 185–207.

Bennett, W.W., Canfield, D.E., 2020. Redox-sensitive trace metals as paleoredox proxies: a review and analysis of data from modern sediments. Earth Sci. Rev. 204.

Berndt, C., Hensen, C., Mortera-Gutierrez, C., Sarkar, S., Geilert, S., Schmidt, M., Liebetrau, V., Kipfer, R., Scholz, F., Doll, M., Muff, S., Karstens, J., Planke, S., Petersen, S., Böttner, C., Chi, W.-C., Moser, M., Behrendt, R., Fiskal, A., Lever, M.A., Su, C.-C., Deng, L., Brennwald, M.S., Lizarralde, D., 2016. Rifting under steam—How rift magmatism triggers methane venting from sedimentary basins. Geology 44, 767–770.

Bray, N., 1988. Water mass formation in the Gulf of California. J. Geophys. Res.: Oceans 93, 9223–9240.

Brumsack, H.-J., 2006. The trace metal content of recent organic carbon-rich sediments: implications for cretaceous black shale formation. Palaeogeogr. Palaeoclimatol. Palaeoecol. 232, 344–361.

Cui, M., Luther, G.W., Gomes, M., 2021. Cycling of W and *Mo species* in natural sulfidic waters and their sorption mechanisms on MnO_2 and implications for paired W and Mo records as a redox proxy. Geochim. Cosmochim. Acta 295, 24–48.

Dellwig, O., Wegwerth, A., Schnetger, B., Schulz, H., Arz, H.W., 2019. Dissimilar behaviors of the geochemical twins W and Mo in hypoxic-euxinic marine basins. Earth Sci. Rev. 193, 1–23.

Eroglu, S., Scholz, F., Frank, M., Siebert, C., 2020. Influence of particulate versus diffusive molybdenum supply mechanisms on the molybdenum isotope composition of continental margin sediments. Geochim. Cosmochim. Acta 273, 51–69.

Firdaus, M.L., Norisuye, K., Nakagawa, Y., Nakatsuka, S., Sohrin, Y., 2008. Dissolved and labile particulate Zr, Hf, Nb, Ta, Mo and W in the western North Pacific Ocean. J. Oceanogr. 64, 247–257.

Fleischmann, S., Du, J., Chatterjee, A., McManus, J., Iyer, S.D., Amonkar, A., Vance, D., 2023. The nickel output to abyssal pelagic manganese oxides: a balanced elemental and isotope budget for the oceans. Earth Planet. Sci. Lett. 619.

Fujiwara, Y., Tsujisaka, M., Takano, S., Sohrin, Y., 2020. Determination of the tungsten isotope composition in seawater: the first vertical profile from the western North Pacific Ocean. Chem. Geol. 555, 119835.

Hein, J.R., Koschinsky, A., Halbach, P., Manheim, F.T., Bau, M., Kang, J.-K., Lubick, N., 1997. Iron and manganese oxide mineralization in the Pacific. Geological Society, London. Special Publ. 119, 123–138.

Iwai, T., Hashimoto, Y., 2017. Adsorption of tungstate (WO 4) on birnessite, ferrihydrite, gibbsite, goethite and montmorillonite as affected by pH and competitive phosphate (PO 4) and molybdate (MoO 4) oxyanions. Appl. Clay. Sci. 143, 372–377.

Kashiwabara, T., Kubo, S., Tanaka, M., Senda, R., Iizuka, T., Tanimizu, M., Takahashi, Y., 2017. Stable isotope fractionation of tungsten during adsorption on Fe and Mn (oxyhydr)oxides. Geochim. Cosmochim. Acta 204, 52–67.

Kashiwabara, T., Takahashi, Y., Marcus, M.A., Uruga, T., Tanida, H., Terada, Y., Usui, A., 2013. Tungsten species in natural ferromanganese oxides related to its different behavior from molybdenum in oxic ocean. Geochim. Cosmochim. Acta 106, 364–378.

Kendall, B., Dahl, T.W., Anbar, A.D., 2017. The stable isotope geochemistry of molybdenum. Rev. Mineral. Geochem. 82, 683–732.

Kishida, K., Sohrin, Y., Okamura, K., Ishibashi, J.-i., 2004. Tungsten enriched in submarine hydrothermal fluids. Earth Planet. Sci. Lett. 222, 819–827.

Kraemer, T., Schornick, J.C., 1974. Comparison of elemental accumulation rates between ferromanganese deposits and sediments in the South Pacific Ocean. Chem. Geol. 13, 187–196.

Kurzweil, F., Archer, C., Wille, M., Schoenberg, R., Münker, C., Dellwig, O., 2021. Redox control on the tungsten isotope composition of seawater. Proceed. National Acad. Sci. 118, e2023544118.

Kurzweil, F., Dellwig, O., Wille, M., Schoenberg, R., Arz, H.W., Münker, C., 2022. The stable tungsten isotope composition of sapropels and manganese-rich sediments from the Baltic Sea. Earth Planet. Sci. Lett. 578, 117303.

Kurzweil, F., Münker, C., Tusch, J., Schoenberg, R., 2018. Accurate stable tungsten isotope measurements of natural samples using a ^{180}W - ^{183}W double-spike. Chem. Geol. 476, 407–417.

Marinone, S.G., 2003. A three-dimensional model of the mean and seasonal circulation of the Gulf of California. J. Geophys. Res. 108.

Mazza, S.E., Gaschnig, R.M., Rudnick, R.L., Kleine, T., 2024. Tungsten stable isotope composition of the upper continental crust. Geochim. Cosmochim. Acta.

Mohajerin, T.J., Helz, G.R., Johannesson, K.H., 2016. Tungsten–molybdenum fractionation in estuarine environments. Geochim. Cosmochim. Acta 177, 105–119.

Peacock, C.L., Moon, E.M., 2012. Oxidative scavenging of thallium by birnessite: explanation for thallium enrichment and stable isotope fractionation in marine ferromanganese precipitates. Geochim. Cosmochim. Acta 84, 297–313.

Post, J.E., 1999. Manganese oxide minerals: crystal structures and economic and environmental significance. Proceed. National Acad. Sci. 96, 3447–3454.

Reifenröther, R., Münker, C., Paulick, H., Scheibner, B., 2022. Alteration of abyssal peridotites is a major sink in the W geochemical cycle. Geochim. Cosmochim. Acta 321, 35–51.

Reifenröther, R., Münker, C., Scheibner, B., 2021. Evidence for tungsten mobility during oceanic crust alteration. Chem. Geol. 584.

Roué, L., Kurzweil, F., Wille, M., Wegwerth, A., Dellwig, O., Münker, C., Schoenberg, R., 2021. Stable W and Mo isotopic evidence for increasing redox-potentials from the paleoarchean towards the paleoproterozoic deep Ocean. Geochim. Cosmochim. Acta 309, 366–387.

Rudnick, R.L., Gao, S., 2014. 4.1 - Composition of the continental crust. In: Holland, H. D., Turekian, K.K. (Eds.), Treatise On Geochemistry, 2nd Edition. Elsevier, Oxford, pp. 1–51.

Scholz, F., 2018. Identifying oxygen minimum zone-type biogeochemical cycling in Earth history using inorganic geochemical proxies. Earth Sci. Rev. 184, 29–45.

Scholz, F., Schmidt, M., Hensen, C., Eroglu, S., Geilert, S., Gutjahr, M., Liebetrau, V., 2019. Shelf-to-basin iron shuttle in the Guaymas Basin, Gulf of California. Geochim. Cosmochim. Acta 261, 76–92.

Sen Tuna, G., Braida, W., 2014. Evaluation of the adsorption of mono- and polytungstates onto different types of clay minerals and pahokee peat. Soil and sediment contamination. Int. J. 23, 838–849.

Simoneit, B.R.T., Kawka, O.E., Brault, M., 1988. Origin of gases and condensates in the Guaymas Basin hydrothermal system (Gulf of California). Chem. Geol. 71, 169–182.

Sohrin, Y., Isshiki, K., Kuwamoto, T., Nakayama, E., 1987. Tungsten in north pacific waters. Mar. Chem. 22, 95–103.

Thunell, R.C., 1998. Seasonal and annual variability in particle fluxes in the Gulf of California: a response to climate forcing. Deep Sea Res. Part I: Oceanographic Res. Papers 45, 2059–2083.

Tribovillard, N., Algeo, T.J., Lyons, T., Riboulleau, A., 2006. Trace metals as paleoredox and paleoproductivity proxies: an update. Chem. Geol. 232, 12–32.
Tsujisaka, M., Nishida, S., Takano, S., Murayama, M., Sohrin, Y., 2020. Constraints on redox conditions in the Japan Sea in the last 47,000 years based on Mo and W as palaeoceanographic proxies. Geochem J 54, 351–363.
van Hulten, M., Middag, R., Dutay, J.-C., de Baar, H., Roy-Barman, M., Gehlen, M., Tagliabue, A., Sterl, A., 2017. Manganese in the west Atlantic Ocean in the context of the first global ocean circulation model of manganese. Biogeosciences 14, 1123–1152.
Wasylenki, L.E., Rolfe, B.A., Weeks, C.L., Spiro, T.G., Anbar, A.D., 2008. Experimental investigation of the effects of temperature and ionic strength on Mo isotope fractionation during adsorption to manganese oxides. Geochim. Cosmochim. Acta 72, 5997–6005.
Yang, R., Li, T., Stubbs, D., Chen, T., Liu, S., Kemp, D.B., Li, W., Yang, S., Chen, J., Elliott, T., Dellwig, O., Chen, J., Li, G., 2022. Stable tungsten isotope systematics on the Earth's surface. Geochim. Cosmochim. Acta 322, 227–243.
Yang, R., Stubbs, D., Elliott, T., Li, T., Chen, T., Paytan, A., Kemp, D.B., Ling, H., Chen, J., Hein, J.R., Coath, C.D., Li, G., 2023. Stable tungsten isotopic composition of seawater over the past 80 million years. Geology 51, 728–732.